JPE 17-4-6

https://doi.org/10.6113/JPE.2017.17.4.905
ISSN(Print): 1598-2092 / ISSN(Online): 2093-4718

Design of a Novel Integrated L-C-T for PSFB ZVS Converters

Jiashen Tian†, Junxia Gao*, and Yiming Zhang*

†,*Faculty of Information, Beijing University of Technology, Beijing, China

Abstract

To enhance the zero-voltage switching (ZVS) range and power density of the phase-shift full-bridge (PSFB) ZVS converters used in geophysical exploration, an additional resonant inductor is used as a leakage inductance and a blocking capacitor which is equivalent to interlayer capacitance is integrated into a novel integrated inductor-capacitor-transformer (L-C-T). The leakage inductance and equivalent interlayer capacitance of the novel integrated L-C-T are difficult to determine by conventional methods. To address this issue, this paper presents accurate and efficient methods to compute the leakage inductance and equivalent interlayer capacitance. Moreover, the accuracy of this methodology, which is based on electromagnetic energy and Lebedev's method, is verified by an experimental analysis and a finite element analysis (FEA). Taking the problems of the novel integrated L-C-T into consideration, the losses of the integrated L-C-T are analyzed and the temperature rise of the integrated L-C-T is determined by FEA. Finally, a PSFB ZVS converter prototype with the novel integrated L-C-T is designed and tested.

Key words: Electromagnetic energy, Equivalent interlayer capacitance, Integrated L-C-T, Lebedev's method, Leakage inductance, ZVS

I. INTRODUCTION

In soft-switching technology, the switching losses of electronic devices can be reduced, so that high-power DC-DC converter can achieve a high-frequency [1]-[3]. However, the primary windings of the transformers in soft-switching converters typically require a series resonant inductor and a blocking capacitor, which increases the size and weight of the transformers [4]-[5]. Through rational design of the magnetic circuit and structure, the resonant inductor and blocking capacitor can be integrated into the transformer [6]-[8]. The integration of passive devices has become one of the core technologies, which further improves the power density of DC-DC converters.

The proposed phase-shift full-bridge (PSFB) zero-voltage switching (ZVS) converter, which is applied for electric geological prospecting, is required to reach ZVS under a light-load and to output 40 kW under a heavy-load. Consequently, the integrated L-C-T in the proposed converter should have enough stray capacitance to absorb the DC harmonics, and have enough leakage inductance to replace the resonant inductor. Various methods for integrating capacitance and leakage inductance into a transformer, which are based on the planar winding and the leakage layer, have been presented in the literature [9]-[12]. However, since a cross-section of the planar windings is usually perpendicular to the leakage magnetic flux of the transformer, the eddy current effect of the planar windings is clearly enhanced [8]. Furthermore, the planar windings and leakage layers are not suitable for high-power, high-frequency transformers.

To overcome these drawbacks, a novel integrated L-C-T has been designed, which consists of copper foil primary windings and separated windings [9]-[12]. At the same time, these parts can ensure the integrity of the primary winding and facilitate the integration of the blocking capacitor. The separated secondary windings of the novel integrated L-C-T are used to increase the leakage inductance. Since the structure of the novel integrated L-C-T is complex, it is difficult to determine the leakage inductance and equivalent interlayer capacitance [4]. Additionally, since the resonant inductor and DC blocking capacitor are integrated into the novel integrated L-C-T, the loss density and temperature rise of the integrated components seriously increase.

To address these problems, methods based on electric field

Manuscript received Jan. 3, 2017; accepted May 12, 2017
Recommended for publication by Associate Editor Il-Oun Lee.
†Corresponding Author: tian_jiashen@126.com
Tel: +86-10-6739-6621, Fax: +86-10-6739-6621, Beijing Univ. of Tech.
*Faculty of Information, Beijing University of Technology, China

energy, magnetic field energy and Lebedev's equations are developed in this paper to determine the leakage inductance and interlayer capacitance of the proposed integrated L-C-T [13]-[15]. In addition, the theoretical analysis is verified by finite element analysis (FEA) and experimental measurements. Furthermore, the loss of the novel integrated L-C-T is analyzed, and the actual operating temperature is calculated by FEA. Finally, a prototype of the novel integrated L-C-T is tested on the proposed PSFB ZVS converter, and its performance is verified.

II. The Structure and Characteristics of the Novel Integrated L-C-T

The novel integrated L-C-T is used in a PSFB ZVS converter for geophysical equipment, which provides a high-voltage, high current signal to the Earth. In addition, the topology of proposed converter is shown in Fig. 1. A conventional transformer plays the roles of power transmitter and voltage converter in the proposed converter. The resonant inductor resonates with parallel capacitors (C_1-C_4) across the insulated-gate bipolar transistors (IGBTs). This is done to ensure the IGBTs achieve ZVS. The circuit configuration of proposed converter is based on the conventional PSFB converter. In addition, C_1=C_2, C_3=C_4, and $\alpha^2 L_{out} >> L_{lk}$, where L_{out} is the output filter inductor, L_{lk} is the leakage inductance of the novel integrated L-C-T, and α is the turns ratio of the L-C-T. The blocking capacitor C_b can eliminate the DC bias of the transformer in the novel integrated L-C-T. Through analysis and design, the resonant inductor, blocking capacitor and transformer in the proposed PSFB ZVS converter can be replaced by the novel integrated L-C-T [16]-[20].

The primary windings n_{pri} are all wound around the center leg, as shown in Fig. 2. EPCOS dielectric films are applied between the primary windings, while the blocking capacitor can be replaced by the equivalent interlayer capacitance between the primary windings and the EPCOS films. The secondary windings are separated into two parts to reduce the voltage stress of the secondary rectifier diodes. Additionally, the secondary windings n_{s11} and n_{s21} are wound around the center column, while the secondary windings n_{s12} and n_{s22} are wound around the side column. Since the primary and secondary windings are not around in the same column, the leakage inductance of the novel integrated L-C-T is sufficient to replace the resonant inductor.

III. Integration of the Blocking Capacitor

In order to integrate the blocking capacitor into the primary windings of the transformer, the primary windings of the novel integrated L-C-T are made out of a flexible multi-layer. The detailed structure of the proposed primary windings is shown in Fig. 3. As shown in Fig. 3(b), a lumped capacitance can be formed between the two primary layers, especially

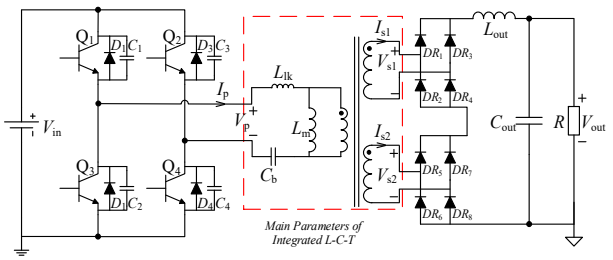

Fig. 1. Main parameters of the PSFB ZVS converter.

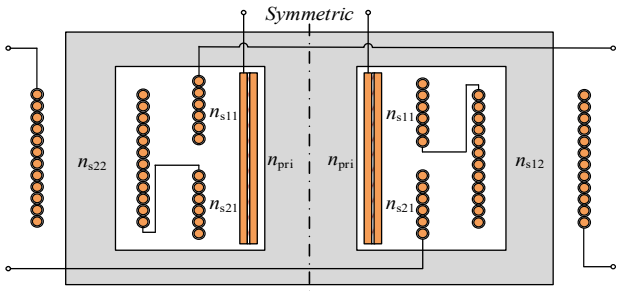

Fig. 2. Main structure of the novel integrated L-C-T.

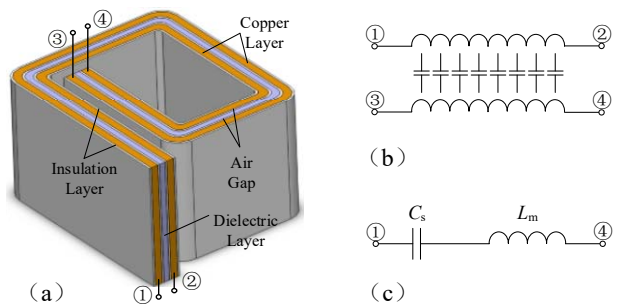

Fig. 3. Structure of the primary winding for the novel integrated L-C-T.

when considering that the EPCOS dielectric layer is sandwiched between the two primary layers. While terminals 2 and 3 are floating and terminals 1 and 4 are used as the primary windings of the transformer, the stray capacitance C_s of the primary windings forms a series relation with the excitation inductance L_m, as shown in Fig. 3(c).

A. Calculation of the Static Interlayer Capacitance

To obtain the equivalent interlayer capacitance C_b' of the primary windings, it is necessary to calculate the static interlayer capacitance C_b. The static interlayer capacitance C_b of the novel integrated L-C-T is composed of the capacitances C_{ins} and C_{die}, as expressed in equation (1), where the static capacitance C_{ins} between the insulating layer and the copper layer is given by equation (2), and the static capacitance between the dielectric layer and the copper layer C_{die} is given by equation (3). Due to air gaps between the flexible multi-layer foils, the actual permittivities are different from the permittivities of the dielectric and insulating layers, and the equivalent methods are stated as shown in equations (4) and (5) [21], [22].

$$C_b = C_{ins} + C_{die} \tag{1}$$

$$C_{die}=\frac{\varepsilon_0\varepsilon'_{die}l_{pri}n_{pri}w_{pri}}{t_{die}+2t_{air}} \tag{2}$$

$$C_{ins}=\frac{\varepsilon_0\varepsilon'_{ins}l_{pri}n_{pri}w_{pri}}{t_{ins}+3t_{air}} \tag{3}$$

$$\varepsilon'_{die}=\frac{\varepsilon_{die}\cdot(t_{die}+2t_{air})}{t_{die}+\varepsilon_{die}\cdot 2t_{air}} \tag{4}$$

$$\varepsilon'_{ins}=\frac{\varepsilon_{ins}\cdot(t_{ins}+3t_{air})}{t_{ins}+\varepsilon_{ins}\cdot 3t_{air}} \tag{5}$$

where, $\varepsilon'_{\text{die}}$ represents the equivalent permittivity of the dielectric film, $\varepsilon'_{\text{ins}}$ denotes the equivalent permittivity of the insulating film, ε_0 indicates the permittivity of the vacuum, l_{pri} is the average length of the primary turns, n_{pri} is the turns of the primary, w_{pri} is the average width of the foil windings, t_{die} is the average thickness of the dielectric films, t_{ins} is the average thickness of the insulating layer, and t_{air} is the equivalent thickness of the air gap.

B. Calculation of the Equivalent Interlayer Capacitance

The static interlayer capacitance is related to the winding structure and winding materials. However, it is not related to the voltage distribution of windings. In addition, the actual distribution of the charges depends on the voltage distribution of the windings. Accordingly, the equivalent interlayer capacitance of the novel integrated L-C-T primary windings is dependent on both the structure and voltage distribution of the winding. The corresponding stored electrostatic energy between the primary layers is given by the following equation:

$$\begin{aligned}W_{\varepsilon}&=\frac{1}{2}\iiint_V D\cdot E dV\\&=W_{die}+W_{ins}\\&=\frac{1}{2}C_{die}V_{Cb}^2+\frac{1}{2}C_{ins}V_{Cb}^2\end{aligned} \tag{6}$$

where, W_{die} is the stored electric energy in the dielectric films, and W_{ins} is the stored electric energy in the insulating films.

To facilitate the calculation, it can be assumed that the transformer magnetic field distribution is uniform and that the voltage in the winding is evenly distributed. Since the two plates of C_{die} belong to the same number of turns, the voltage across C_{die} is V_{Cb}. The palates of C_{ins} belong to different turns of the primary windings. Therefore, the voltage across C_{ins} is $V_{\text{Cb}}+(V_{\text{in}}-V_{\text{Cb}})/n_{\text{pri}}$. According to the winding structure in Fig 3(a), the electric fields of C_{die} and C_{ins} are given by the equation:

$$\begin{cases}E_{die}(x)=\dfrac{V_{Cb}}{t_{die}+2t_{air}}\\[2ex]E_{ins}(x)=\dfrac{V_{in}+(n_{pri}-1)V_{Cb}}{(t_{ins}+3t_{air})\cdot n_{pri}}\end{cases} \tag{7}$$

where, V_{Cb} is the voltage across the blocking capacitance, and V_{in} is the input voltage.

Thus, W_{die} is given by the equation:

$$\begin{aligned}W_{die}&=\frac{1}{2}\iiint_V\varepsilon_0\varepsilon'_{die}E_{die}^2(x)dV\\&=\frac{1}{2}\frac{\varepsilon_0\varepsilon'_{die}l_{pri}w_{pri}V_{Cb}^2}{(t_{die}+2t_{air})}\\&=\frac{1}{2}C'_{die}V_{Cb}^2\end{aligned} \tag{8}$$

In addition, W_{ins} is given by the following equation:

$$\begin{aligned}W_{ins}&=\frac{1}{2}\iiint_V\varepsilon_0\varepsilon'_{ins}E_{ins}^2(x)dV\\&=\frac{1}{2}\frac{\varepsilon_0\varepsilon'_{ins}l_{pri}w_{pri}\left[V_{in}+(n_{pri}-1)V_{Cb}\right]^2}{(t_{ins}+3t_{air})\cdot n_{pri}^2}\\&=\frac{1}{2}C_{ins}\frac{\left[V_{in}+(n_{pri}-1)V_{Cb}\right]^2}{n_{pri}^2}\\&=\frac{1}{2}C'_{ins}V_{Cb}^2\end{aligned} \tag{9}$$

where C_{ins}' is the equivalent interlayer capacitance of the insulation, and C_{die}' is the equivalent interlayer capacitance of the dielectric.

Based on the stored electric energy, the equivalent interlayer capacitance of the novel integrated L-C-T primary layers can be expressed as follows:

$$\begin{cases}C'_{die}=C_{die}\\[2ex]C'_{ins}=\dfrac{\left[V_{in}+(n_{pri}-1)V_{Cb}\right]^2}{n_{pri}^2V_{Cb}^2}C_{ins}\end{cases} \tag{10}$$

Assuming that the voltage across the blocking capacitance $V_{\text{Cb}} = 0.1V_{\text{in}}$, as previously those described [23]. Then the equivalent capacitance is as follows:

$$C'_{ins}=\frac{\left(n_{pri}+9\right)^2}{n_{pri}^2}C_{ins} \tag{11}$$

The equivalent interlayer capacitance is expressed as:

$$\begin{aligned}C'_b&=C'_{die}+C'_{ins}\\&=\frac{\varepsilon_0\varepsilon'_{die}l_{pri}n_{pri}w_{pri}}{t_{die}+2t_{air}}+\frac{\left(n_{pri}+9\right)^2}{n_{pri}^2}\cdot\frac{\varepsilon_0\varepsilon'_{ins}l_{pri}n_{pri}w_{pri}}{t_{ins}+3t_{air}}\end{aligned} \tag{12}$$

IV. Integration of the Resonant Inductor

The novel integrated L-C-T with separated secondary windings is presented in Fig. 2. Since the primary and secondary windings are not wound around the same column, the linkage of the windings decreases and the leakage flux increases. The flux distribution of the novel integrated L-C-T is presented in Fig. 4, where Φ_0, Φ_1 and Φ_2 are the main fluxes, Φ_{in} is the inner leakage flux, Φ_{eq} is the equivalent leakage flux, and Φ_{y} is the yoke leakage flux. Half of the leakage inductance consists of three components, namely the inner leakage inductance L_{in}, the yoke leakage inductance L_{y}, and the equivalent leakage inductance L_{eq}. Due to the

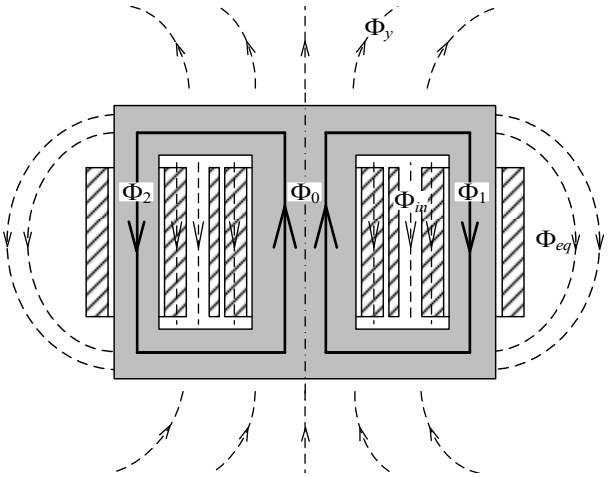

Fig. 4. Flux distribution of the novel integrated L-C-T.

symmetry of the novel integrated L-C-T, the leakage inductance of the novel integrated L-C-T is expressed as follows:

$$L_{\mathrm{lk}} = 2(L_{\mathrm{in}} + L_{\mathrm{y}} + L_{\mathrm{eq}}) \tag{13}$$

A. Calculation of the Inner Leakage Inductance

Since the novel integrated L-C-T is not designed by conventional methods, an empirical formula is not suitable for calculating the value of L_{in} for the novel integrated L-C-T. In addition, since a prototype is needed to obtain L_{in} through measurements, the design process of the novel integrated L-C-T is slowed down. Consequently, stored magnetic energy is used to determine the inner leakage inductance L_{in}, which is simpler and more accurate than other methods.

The inner leakage flux density of the half-core window is shown in Fig. 5, where $H(x)$ is the magnetic flux density of the inner leakage field, $H(max)$ is the maximum flux density of the inner field, and $H(mid)$ is the middle flux density of the inner field. At stage t_1-t_2, the flux density increases from zero to $H(max)$, because n_{pri} is turned around the center leg of the core. At stage t_2-t_3, the flux density is kept at $H(max)$, due to the insulation between the primary and secondary windings of the transformer. At stage t_3-t_4, since some of the secondary windings (n_{s11} and n_{s21}) are turned around the center leg of the core, $H(x)$ decreases quickly. At stage t_4-t_5, the magnetic field remains at $H(mid)$, because of the air between the center leg and the side leg of the core. At stage t_5-t_6, $H(x)$ decreases to zero, due to n_{s12} being around the side leg of the core. According to the principle of magnetic energy, plenty of energy is stored in the leakage magnetic field at stage t_1-t_6. In addition, the magnetic energy storage of the inner leakage field increases with the number of n_{s12}.

The energy of the inner leakage field W_{in} can be expressed as follows:

$$W_{in} = \frac{\mu_0}{2}\int H(x)^2 dv \tag{14}$$

The magnetic field distribution is shown in Fig. 5, and the

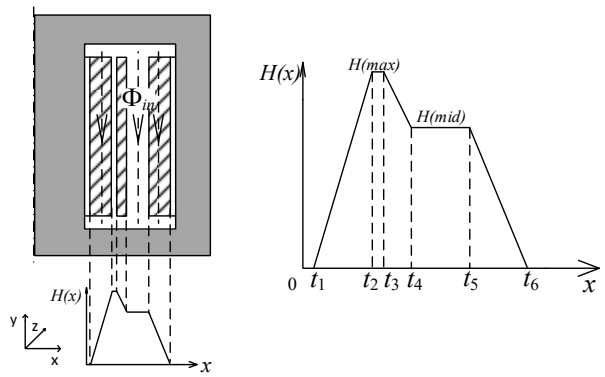

Fig. 5. Inner leakage flux density of the half-core window.

TABLE I
CALCULATION OF THE STORED MAGNETIC ENERGY IN THE INNER LEAKAGE FIELDS

Internal	The stored energy
t_1-t_2	$W_{\mathrm{in\_1}} = \frac{1}{2}\mu_0 l_w h_w \int_0^{t_2-t_1}\left[\frac{n_{pri}I_{pri}}{(t_2-t_1)h_{\mathrm{w}}}x\right]^2 dx$
t_2-t_3	$W_{\mathrm{in\_2}} = \frac{1}{2}\cdot\frac{\mu_0 l_{\mathrm{w}} n_{pri}^2 I_{pri}^2}{h_{\mathrm{w}}}(t_3-t_2)$
t_3-t_4	$W_{\mathrm{in\_3}} = \frac{1}{2}\mu_0 l_w h_w \int_0^{t_4-t_3}\left(\frac{n_{pri}I_{pri}-\frac{n_{s11}I_{sec}}{t_4-t_3}x}{h_w}\right)^2 dx$
t_4-t_5	$W_{in\_4} = \frac{1}{2}\mu_0 l_w h_w\left(\frac{n_{pri}I_{pri}-n_{s11}I_{sec}}{h_w}\right)^2(t_5-t_4)$
t_5-t_6	$W_{\mathrm{in\_5}} = \frac{1}{2}\mu_0 l_w h_w \int_{t_5}^{t_6}\left[-\frac{\frac{n_{s21}I_{sec}}{t_6-t_5}(x-t_6)}{h_w}\right]^2 dx$

stored magnetic energy W_{in} can be calculated as follows [12], [13]:

$$W_{in} = \frac{1}{2}\mu_0 l_w h_w \sum_{i=1}^{6}\int_{t_{i-1}}^{t_i} H_i(x)^2 dx \tag{15}$$

where, μ_0 is the permeability of the vacuum, l_{w} is the width of the core window along the z axis, and h_{w} is the height of the core window.

The stored magnetic energy in each stage of the inner leakage field can be expressed as shown in Table I, where I_{pri} is the peak current of the primary windings, and I_{sec} is the peak current of the secondary windings.

In summary, the inner leakage inductance of the novel integrated L-C-T is as follows:

$$L_{in} = \frac{\sum_{a=1}^{5} W_{in\_a}}{I_{pri}^2} \tag{16}$$

B. Calculation of the Yoke Leakage Inductance

The yoke leakage inductance is proportional to the square of n_{s12} [15]. As shown in Equation (17), the yoke leakage

inductance L_{s_y} at the secondary windings is calculated by Lebedev's method [24]. Then the yoke leakage inductance L_y at the primary windings can be calculated by Equation (18):

$$L_{s\_y} = \frac{\mu_0 n_{s12}^2 b_c l_w}{6 h_c} \tag{17}$$

$$L_y = \alpha^2 L_{s\_y} \tag{18}$$

where b_c is the width of the core along the x axis, h_c is the height of the core, and α is the turns ratio of the novel integrated L-C-T.

C. Calculation of the Equivalent Leakage Inductance

The equivalent leakage inductance of the secondary L_{s_eq} is related to the turns of n_{s12}, the average length l_{s12} of n_{s12}, the width of the core window along the x axis b_w, and the height of the core window h_w [25]. In addition, while the core structure is determined, the equivalent leakage inductance L_{eq} is proportional to the square of n_{s12}. Consequently, L_{s_eq} is converted to the primary to get L_{eq}, as shown in the following equations:

$$L_{s\_eq} = \frac{\mu_0 n_{s12}^2 l_{s12} b_w}{3 h_w} \tag{19}$$

$$L_{eq} = \alpha^2 L_{s\_eq} \tag{20}$$

Based on the stored magnetic energy method and Lebedev's method, the leakage inductance of the novel integrated L-C-T can be calculated using Equation (13). The proposed methods are more suitable for the integrated L-C-T with its complex structure.

V. Losses of the Novel Integrated L-C-T

Since the blocking capacitor, the resonant inductor and the transformer are integrated into the novel integrated L-C-T, the size and weight of the proposed device are reduced. On the other hand, the loss density and temperature of the novel integrated L-C-T are increased. To solve the overheating problem of the integrated components, the losses of these components are analyzed in this paper. Due to the serious overheating of the novel integrated L-C-T, necessary cooling measures are adopted. The thermal design is one of the most important parts of the novel integrated L-C-T, and the losses of the proposed L-C-T are discussed in parts A-C.

A. Dielectric Losses

$$P_{Cb} = 2\pi f \cdot C_b' \cdot V_{Cb}^2 \cdot \tan\delta \tag{21}$$

The dielectric loss of the equivalent capacitance is associated with the following factors: the operating frequency f, the voltage across the capacitor V_{Cb}, the equivalent capacitance of the primary C_b', and the small-signal loss factor ($\tan\delta$). The $\tan\delta$ of the dielectric is known by a measurement at 20 kHz.

B. Core Losses

The core losses of the transformer include hysteresis loss, anomalous eddy current loss and eddy current loss. The core losses in the full-bridge circuit are expressed as follows:

$$\begin{aligned} P_{Fe} &= P_h + P_a + P_e \\ &= P_h + k_a B_m^{1.5} f^{1.5} + k_e B_m^2 f^2 \end{aligned} \tag{22}$$

where P_h denotes the hysteresis loss, P_a represents the anomalous eddy current loss, P_e is the eddy current loss, k_a is the coefficient of the anomalous eddy current loss, k_e is coefficient of the eddy current loss, and B_m is the maximum magnetic flux density.

The values of k_a and k_e for different materials are different, The values of k_a and k_e for each sample are shown in Table II. The maximum magnetic flux density of the integrated L-C-T is expressed by the following equations, as previously reported [26]:

TABLE II
Fitting Coefficients of the Proposed Model

Material	K_a	K_e
Nanocrystalline	$1.2\cdot10^{-5}$	$1.8\cdot10^{-7}$
Amorphous	$5.7\cdot10^{-5}$	$7.2\cdot10^{-7}$
6.5% silicon steel sheet	$1.1\cdot10^{-4}$	$4.4\cdot10^{-5}$
3% grain-oriented silicon steel sheet	$2.8\cdot10^{-4}$	$1.3\cdot10^{-5}$

$$B_m = B_{tra} + B_{ind} \tag{23}$$

$$B_{tra} = \frac{V_{in}}{2 A_c K_f n_{pri} f} \tag{24}$$

$$B_{ind} = \frac{L_{lk} I_{pri}^2}{K_u A_p J} \tag{25}$$

where B_{tra} is the maximum magnetic flux density of the transformer, B_{ind} is the maximum magnetic flux density of the inductor, J is the current density of the primary, A_c is the sectional area of the core center leg, A_p is the area product of the core, K_f is the coefficient of the square waveform, and K_u is the occupied area of the core window.

C. Winding Losses

The general winding losses of the transformer can be expressed as:

$$\begin{aligned} P_{Cu} &= I_{pri}^2 R_{pri} + I_{sec}^2 R_{sec} \\ &= I_{pri}^2 \frac{\sigma l_{pri} n_{pri}}{A_{pri}} \left(\frac{R_{ac}}{R_{dc}}\right)_{pri} \\ &\quad + I_{sec}^2 \frac{\sigma l_{sec} n_{sec}}{A_{sec}} \left(\frac{R_{ac}}{R_{dc}}\right)_{sec} \end{aligned} \tag{26}$$

where σ represents the conductivity of copper, l_{pri} is the average length of the primary turns, l_{sec} is the average length of the secondary turns, n_{sec} denotes the turns of the secondary windings, A_{pri} is the equivalent sectional area of the primary windings, and A_{sec} is the equivalent sectional area of the secondary windings.

Generally, Litz line is used to replace the conventional line to eliminate the skin effect. Since the secondary of the novel

TABLE III
INTEGRATED L-C-T PARAMETERS

Parameter	Value
Primary winding	Foil
Secondary winding	Litz line
Dielectric material	Polyimide
Core material	Nanocrystal
Turns ratio(α)	1.25
Area of center leg(A_c)	25cm^2
Area of side leg(A_s)	12.5cm^2
window height(h_w)	10cm
window width along x axis(b_w)	3cm
width along z axis(l_w)	4cm
Mean turn length in primary(l_a)	14cm
Mean turn length in secondary(l_a)	20cm
Dielectric thickness	0.2mm
Insulator thickness(h_t)	0.2mm

integrated L-C-T is made of Litz line, the skin effect of the secondary windings is not considered. On the other hand, the skin effect of the foil windings must be considered. Therefore, the AC factor of the secondary resistance $(R_{ac}/R_{dc})_{sec}$= 1, and the AC factor of the primary resistance is as follows:

$$\left(\frac{R_{ac}}{R_{dc}}\right)_{pri} = y\left[M(y)+\frac{2}{3}(n_{pri}^2-1)D(y)\right] \quad (27)$$

where y denotes d_{foil}/δ, d_{foil} is the foil thickness (m), δ is the skin depth at 20 kHz, $M(y)$ is $(\sinh(2y)+\sin(2y))/(\cosh(2y)-\cos(2y))$, and $D(y)$ is $(\sinh(y)-\sin(y))/(\cosh(y)+\cos(y))$.

VI. FEA VERIFICATIONS AND EXPERIMENTAL RESULTS

The main parameters of the novel integrated L-C-T are presented in Table III. Accordingly, FEA software (ANSYS Maxwell) is adopted to simulate the magnetic field of the novel integrated L-C-T, as shown in Fig. 8. The magnetic field distribution of the novel integrated L-C-T in chapter 2 is verified by FEA, and the leakage inductance of the novel integrated L-C-T is calculated, as shown in Fig. 6. Moreover, a prototype of the novel integrated L-C-T is used to verify the theory. A LCR meter is used to measure the leakage inductance and the interlayer capacitance. A comparison of the leakage inductances determined by the three different methods is presented in Fig. 6, and a comparison of the interlayer capacitances determined by measurement and calculations is shown in Fig. 7. The comparisons in Fig.6 and Fig. 7, reveal that the formulas of the leakage inductance and equivalent interlayer capacitance are accurate and suitable for the novel integrated L-C-T.

To ensure that the proposed PSFB ZVS converter with the

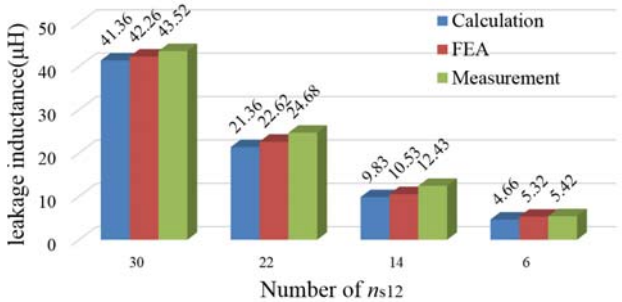

Fig. 6. Comparison of the leakage inductances of three different methods.

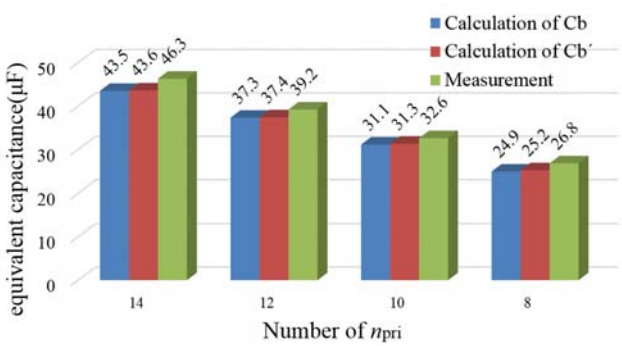

Fig. 7. Comparison of the equivalent capacitances of three different methods.

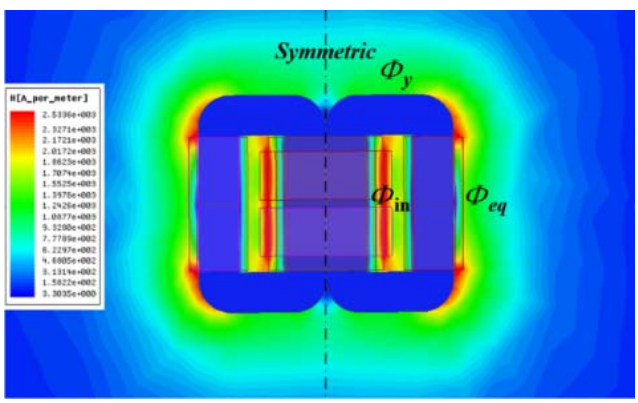

Fig. 8. Magnetic analysis of the novel integrated L-C-T.

integrated L-C-T can achieve soft-switching under a light load, the leakage inductance of the novel integrated L-C-T is more than 20 μH. Moreover, to ensure that the DC magnetic bias of the novel integrated L-C-T is eliminated, the equivalent interlayer capacitance is about 37μF. As shown in Fig. 6 and Fig. 7, a prototype of the novel integrated L-C-T is designed to have 12 turns of n_{pri}, 4 turns of n_{s11}, and 22 turns of n_{s12}. In addition, as shown in Fig. 9, a comparison of the conventional separated components and the proposed integrated L-C-T indicates that the size and weight of the novel integrated L-C-T is half that of the conventional components.

The losses of the novel integrated L-C-T are analyzed in chapter 5. Then FEA software (ANSYS Icepak) is used to simulate a temperature rise of the integrated L-C-T under

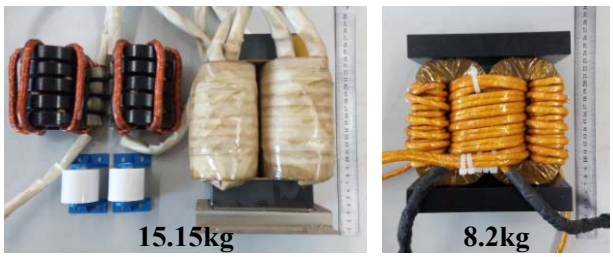

(a) (b)

Fig. 9. Comparison of the conventional separated components and the novel integrated L-C-T: (a) conventional separated components; (b) novel integrated L-C-T.

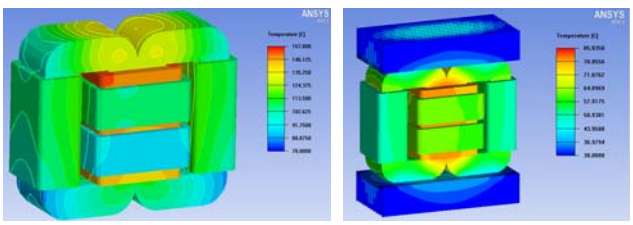

(a) (b)

Fig. 10. Thermal analysis of the novel integrated L-C-T: (a) novel integrated L-C-T with natural air cooling; (b) novel integrated L-C-T with forced air cooling.

high power (40 kW). A temperature simulation of the proposed L-C-T is shown in Fig. 10(a). When the novel integrated L-C-T without the heat–sinks seriously overheats, the maximum temperature reaches 157℃ (the point on the foil windings of the primary), and the minimum temperature reaches 80℃ (the Litz line of the side column). To avoid serious overheating, two heat-sinks (Aluminum alloy 6063) are installed near the top and bottom of the novel integrated L-C-T. Moreover, natural air cooling is used instead of the forced air cooling in the novel integrated L-C-T. The temperature rise of the novel integrated L-C-T with forced air cooling is shown in Fig. 10 (b). After this improvement, the maximum temperature is 85.8 ℃, which is below the maximum permissible temperature for all of the materials of the novel integrated L-C-T.

Finally, to verify the performance of the PSFB ZVS converter with the proposed L-C-T, a prototype with a constant current, variable voltage and 40 kW power is developed, as shown in Fig. 11. The prototype is implemented with the following specifications: input voltage V_{in}= 340—420 V, output voltage V_{out}= 200—1000 V, output current I_{out}= 40 A, switching frequency f= 20 kHz, primary switches Q_1—Q_4=FF300R12KE4, transformer leakage inductance L_{lk}=23.28μH, high-frequency rectifiers DR_1—DR_8= DSEI 2x101, output inductor L_{out}=1.6mH, output capacitor C_{out}= 990μF, and Fan= DB 1238B24H (12V, 21.6W, r/min= 6000). Since it is more difficult for the lagging switch to reach ZVS than the leading switch, ZVS of the lagging switch is the implied ZVS of the proposed converter. Fig. 13 shows waveforms of the lagging switch, where V_{CE} is the

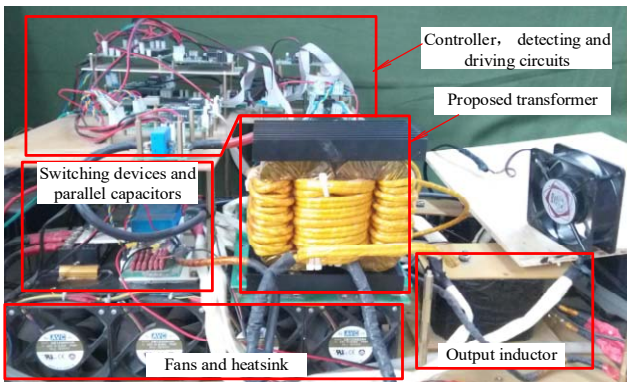

Fig. 11. Prototype of the proposed PSFB ZVS converter.

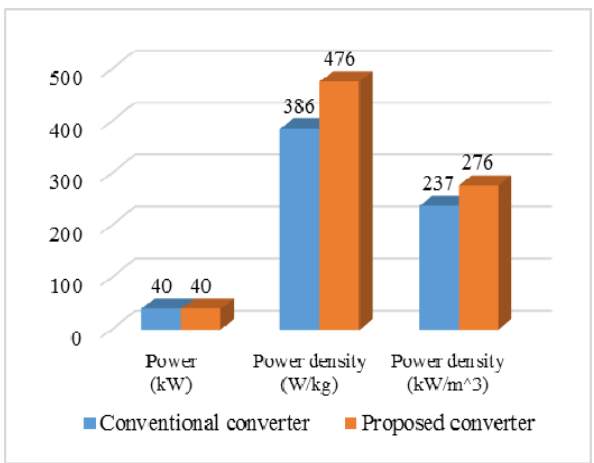

Fig. 12. Power density comparisons of the conventional converter with separated magnetic components and the proposed conventer with the novel integrated L-C-T.

collector-emitter voltage of the lagging switch, and V_{GS} is the gate charge of the lagging switch. Since the lagging switch turns on after V_{CE} drops to zero, and turns off before V_{CE} increases from zero, the lagging switch reaches ZVS. Fig. 14(a) shows waveforms of V_p, I_p and $V_{out1,2}$. It can be seen that $V_{out1,2}$ is zero when V_p becomes 540 V. Apparently, the value of L_{lk} for the proposed L-C-T resonates with the parallel capacitors (C_1-C_4) at that time. I_p flows through the freewheeling diodes of the IGBTs and the primary winding of the L-C-T, while the voltage across lagging switches is clamped to zero. In addition, I_p is 50 A when V_p and $V_{out1,2}$ become zero. In this interval, I_p flows through the primary winding and the freewheeling diodes of the IGBTs, and the leading switch can reach ZVS. There is a certain voltage distortion of the novel integrated L-C-T during the rising phase. However, the proposed converter still achieved soft-switching at a light-load. The waveforms of the proposed converter at a heavy-load are shown in Fig. 14(b). The duty loss of the secondary voltage is within the acceptable range. Fig. 12 shows power density comparisons of the proposed PSFB ZVS converter with the novel integrated L-C-T and the conventional PSFB ZVS converter with separated magnetic components. The novel integrated L-C-T can completely

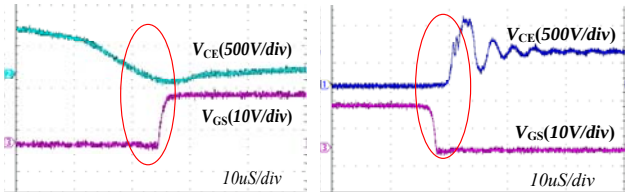

(a) (b)

Fig. 13. Waveforms of the lagging switch: (a) turn-on waveforms; (b) turn-off waveforms.

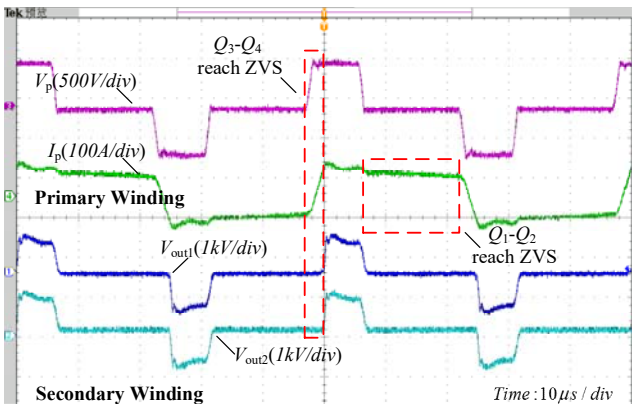

(a)

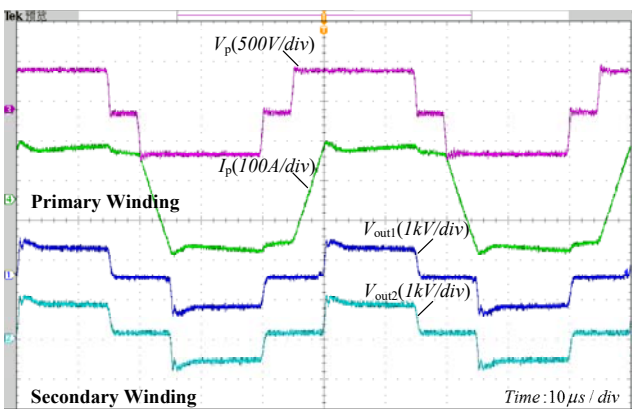

(b)

Fig. 14. Waveforms of the proposed IM transformer: (a) light-load condition; (b) 100% load condition.

replace the separated components in the proposed PSFB ZVS converter, and improve the power density of the converter.

VII. Conclusions

A novel integrated L-C-T, which is suitable for PSFB ZVS converters with high power and high voltage, has been proposed and developed in this paper. Calculation methods for the equivalent interlayer capacitance and leakage inductance of the novel integrated L-C-T are presented and verified by measurements and FEA. By simply setting the turns of the primary and secondary windings, the equivalent interlayer capacitance and leakage inductance of the proposed L-C-T can be easily designed. After a comparison with a conventional transformer, the novel integrated L-C-T is found to decrease the size and weight by half. Additionally, through a suitable thermal design, the temperature rise of the novel integrated L-C-T is limited to an acceptable range. Therefore, the novel integrated L-C-T in this paper is very appropriate for the high power, high power density PSFB ZVS converters.

Acknowledgment

This work was supported by R&D of Instruments and Technologies for Deep Resources Prospecting (the National R&D Projects for Key Scientific Instruments), Grant No. ZDYZ2012-1-05.

References

[1] G. N. B. Yadav and N. L. Narasamma, "An active soft switched phase-shifted full-bridge DC–DC converter: Analysis, modeling, design, and implementation," *IEEE Trans. Power Electron*., Vol. 29, No. 9, pp. 4538-4550, Sep. 2014.

[2] S. H. Lee, C. Y. Park, J. M. Kwon, B.-H. Kwon, "Hybrid-type full-bridge dc/dc converter with high efficiency," *IEEE Trans. Power Electron.*, Vol. 30, No. 8, pp.4156-4164, Aug. 2015.

[3] K. Shi, D. Zhang, Z. Zhou, M. Zhang, and Y. Gu, "A novel phase-shift dual full-bridge converter with full soft-switching range and wide conversion range," *IEEE Trans. Power Electron*., Vol. 31, No.11, pp. 7747-7760, Nov. 2016.

[4] Y. Jiang, Z. Chen, and J. Pan, "Zero-voltage switching phase shift full-bridge step-up converter with integrated magnetic structure," *IET Power Electron.*, Vol. 3, No. 5, pp.732-739, Dec. 2009.

[5] Y. Jang, M. M. Jovanović, and Y. M. Chang, "A new zvs-pwm full-bridge converter," *IEEE Trans. Power Electron*., Vol. 18, No. 5, pp. 232-239, Sep. 2002.

[6] K. U. Member, "A generalized method for lagrangian modeling of power conversion circuit with integrated magnetic components," *IEEJ Trans. Electr. Electron*., Vol. 7, No. S1, pp. 146-152, 2012.

[7] K. Umetani, S. Arimura, T. Hirano, J. Imaoka, M. Yamamoto, "Evaluation of the Lagrangian method for deriving equivalent circuits of integrated magnetic components: A case study using the integrated winding coupled inductor," *IEEE Trans. Ind. Appl.*, Vol. 51, No. 1, pp.547-555, Jan/Feb. 2015.

[8] M. Pahlevani, S. Eren, A. Bakhshai, and P. Jain, "A series-parallel current-driven full-bridge dc/dc converter," *IEEE Trans. Power Electron*., Vol. 31, No. 2, pp. 1275-1293, Feb. 2016.

[9] N. Zhu, J. D. van Wyk, and F. Wang, "Design of integrated parallel resonant transformers," *in IEEE Power Electronics Specialists Conference*, pp. 1787-1792, 2005.

[10] J. T. Strydom, J. D. van Wyk, and J. A. Ferreira, "Some limits of integrated L-C-T modules for resonant converters at 1MHz," *IEEE Trans. Ind. Appl*,. Vol. 37, No. 3, pp. 820-828, May/Jun. 2001.

[11] J. T. Strydom, "Electromagnetic design of integrated resonator-transformers," PhD. Thesis, Rand Afrikaans University, 2001.

[12] W. Liu, "Alternative structures for integrated

electromagnetic passives," PhD. Thesis, Virginia Tech., 2006.
[13] Z. Ouyang, J. Zhang, and W. G. Hurley, "Calculation of leakage inductance for high-frequency transformers," *IEEE Trans. Power Electron*., Vol. 30, No. 10, pp. 5769-5775, Oct. 2015.
[14] M. A. Bahmani and T. Thiringer, "Accurate evaluation of leakage inductance in high-frequency transformers using an improved frequency-dependent expression," *IEEE Trans. Power Electron*., Vol. 30, No. 10, pp. 5738-5745, Oct. 2015.
[15] R. Doebbelin, C. Teichert, M. Benecke, and A. Lindemann, "Computerized calculation of leakage inductance values of transformers," *Piers Online*, Vol. 5, No. 8, pp. 721-726, Aug. 2009.
[16] R. Chen, J. T. Strydom, J. D. van Wyk, "Design of planar integrated passive module for zero-voltage-switched asymmetrical half-bridge PWM converter," *IEEE Trans. on Ind. Appl*., Vol. 39, No. 6, pp. 1648-1655, Nov/Dec. 2003.
[17] I. W. Hofsajer, J. A. Ferreira, J. D. van Wyk, "Design and analysis of planar integrated LCT components for converters," *IEEE Trans. Power Electron*., Vol. 15, No. 6, pp. 1221-1227, Nov. 2000.
[18] M. C. Smit, J. A. Ferreira, J. D. Van Wyk, and M. Ehsani, "An ultrasonic series resonant converter with integrated LCT," *IEEE Trans. Power Electron*., Vol. 10, No. 1, pp. 25-31, Jan. 1995.
[19] P. A. J. van Rensburg, J. D. van Wyk, and J. A. Ferreira, "Design, prototyping and assessment of a 3 kW integrated LCT component for deployment in various resonant converters," *IET Power Electron*., Vol. 2, No. 5, pp. 535-544. Aug. 2008.
[20] Y. Lembeye, P. Goubier, and J. P. Ferrieux, "Integrated planar l-c-t component: design, characterization and experimental efficiency analysis," *IEEE Trans. Power Electron.*, Vol. 20, No. 3, pp. 593-599, May. 2005.
[21] L. Dalessandro, F. S. Cavalcante, and J. W. Kolar, "Self-capacitance of high-voltage transformers," *IEEE Trans. Power Electron.*, Vol. 22, No. 5, pp.2081-2092, Sep. 2007.
[22] J. Biela and J. W. Kolar, "Using transformer parasitics for resonant converters-A review of the calculation of the stray capacitance of transformers," *IEEE Trans. Ind. Appl.*, Vol. 44, No. 1, pp.223-233, Jan. 2008.
[23] A. Pressman, *Switching Power Supply Design*, Chap.3, McGraw-Hill, 2009.
[24] V. K. Lebedev, "Calculation of the short-circuit resistance of welding transformers with yoke leakage (russ.)," *Automatic Welding*, Vol. 11, No. 4, pp. 37-44, 1958.
[25] R. Doebbelin, M. Benecke, and A. Lindemann, "Calculation of leakage inductance of core-type transformers for power electronic circuits," *in Proc. Power Electronics and Motion Control Conf*., pp. 1280-1286, 2008.
[26] C. W. T. Mclyman, *Transformer and Inductor Design Handbook*, Chap.7/8, M. Dekker, 1978.

Jiashen Tian was born in Beijing, China, in 1990. He received his B.S. degree from the College of Electrical and Electronic Engineering, North China Institute of Science and Technoloigy, Hebei, China, in 2012; and his M.S. degree from the Faculty of Information, Beijing University of Technology, Beijing, China, in 2015, where he is presently working towards his Ph.D. degree. He is participating in research dealing with the quality control of electrical equipment, electric tests and tests on the electromagnetic compatibility of electrical and electronic equipment. His current research interests include the modeling and control of switching power supplies, magnetic components, system optimization concerning electromagnetic fields and high voltages.

Junxia Gao was born in Tianjin, China, in 1978. She received her B.S. degree from the College Information Engineering, Taiyuan University of Technology, Taiyuan, China, in 2001; and her M.S. degree from the Faculty of Information, Beijing University of Technology, Beijing, China, in 2004. Since 2004, she has been a Senior Lecturer in the Faculty of Information, Beijing University of Technology. Her current research interests include power electronics, electromagnetic fields and nondestructive examination.

Yiming Zhang was born in Hubei, China, in 1964. He received his B.S. degree from the School of Electronic, Information and Electrical Engineering, Shanghai Jiao Tong University, Shanghai, China, in 1988; and his M.S. degree from the School of Electrical Engineering and Automation, Harbin Institute of Technology, Harbin, China, in 1992. From 2000 to 2007, he was a Senior Researcher in the Institute of Electrical Engineering, Chinese Academy of Sciences, Beijing, China. Since 2008, he has been an Professor in the College of Electronic Information and Control Engineering, Beijing University of Technology, Beijing, China. His current research interests include intelligent power management, motor speed control, servo drivers and motor energy conservation.